Lorentz near-field electron ptychography

View Online   Export Citation   CrossMark

Shengbo You,[1,a)] (iD) Peng-Han Lu,[2] (iD) Thomas Schachinger,[3,4] (iD) András Kovács,[2] (iD) Rafal E. Dunin-Borkowski,[2] (iD) and Andrew M. Maiden[1,5] (iD)

AFFILIATIONS

[1]Department of Electronic and Electrical Engineering, University of Sheffield, Sheffield S1 4DE, United Kingdom
[2]Ernst Ruska-Centre for Microscopy and Spectroscopy with Electrons and Peter Grünberg Institute, Forschungszentrum Juelich, 52425 Juelich, Germany
[3]Institute of Solid State Physics, TU Wien, 1040 Wien, Austria
[4]University Service Centre for Transmission Electron Microscopy, TU Wien, 1040 Wien, Austria
[5]Diamond Light Source, Diamond House, Harwell Science and Innovation Campus, Didcot OX11 0DE, United Kingdom

[a)]Author to whom correspondence should be addressed: syou1@sheffield.ac.uk

ABSTRACT

Over the past few years, electron ptychography has drawn considerable attention for its ability to recover high contrast and ultra-high resolution images without the need for high quality electron optics. In this Letter, we focus on electron ptychography's other potential benefits: quantitatively mapping phase variations resulting from magnetic and electric fields over extended fields of view. To this end, we propose an implementation of near-field ptychography that employs an amplitude mask located in the electron microscope's condenser aperture plane. We demonstrate the capabilities of our method by imaging a magnetic Permalloy sample and compare our results with those of off-axis electron holography.

Ptychography is a computational imaging method that is becoming widely used in electron microscopy. In its conventional form, it is a type of scanned-probe microscopy, in which a convergent electron beam—the ptychographic probe—illuminates a small patch of a sample and then scans through a grid of positions to cover a region of interest, recording diffraction patterns at each point in the grid. The diffraction patterns are processed by iterative algorithms to reconstruct an image of the complex-valued transmission function of the sample while simultaneously recovering the probe wavefront.[1] This simple experimental process, coupled with robust reconstruction algorithms, has led to ptychography's uptake across a range of wavelengths, from visible light[2,3] to x-rays[4–6] and electrons.[7–12] However, due to the near-focused probe and the requirement for significant overlap of the scan positions, covering a large field of view using ptychography is problematic; it requires collection of many diffraction patterns, often numbering in the tens of thousands, which is time-consuming both in terms of data collection and data processing. Near-field electron ptychography replaces the conventional focused electron beam with a full-field, structured illumination and repositions the detector so that it records near-field (Fresnel region) rather than far-field diffraction patterns. At the expense of a drop in the achievable resolution

(limited now by the electron optics), it provides quantitative phase images over large fields of view, from data comprising tens not thousands of diffraction patterns.

Near-field ptychography was first demonstrated with x-rays[13,14] but has since been extended to visible light[15] and electron[16,17] microscopy. In the first electron implementation,[16] the sample was illuminated by a broad, roughly parallel illumination beam, and the microscope's selected area aperture (SAA) was used to choose a region of interest from the resulting brightfield image. The SAA acted like a virtual probe; it can be thought of as equivalent to the sample being illuminated by an electron beam shaped like the aperture, shrunk down by the magnification factor of the microscope objective lens. This method was later improved by inserting an engineered phase plate (or diffuser) in the SAA[17] to better modulate the sample image wavefront. The diffuser added interference fringes to the data, supplementing diffraction from the aperture edges such that even large apertures covering a large sample area produced data containing plenty of fringe structure. This highly structured data meant megapixel phase images could be reconstructed from as few as nine diffraction patterns, but while it considerably reduced the data requirements over the original method, this diffuser-based implementation did not make efficient

use of dose, since sample areas outside of the region masked by the SAA were constantly exposed to the beam, and signal was lost through inelastic scatter from the phase plate. Changing the magnification of the setup to image at different resolutions was also difficult. It required a different size of SAA for each magnification, so that a full set of diffuser-equipped apertures was required for multi-scale imaging.

The method we present in this Letter overcomes these limitations through an experimental arrangement in which the diffuser is located in the condenser aperture, as shown in Fig. 1. Moving the diffuser from the SAA to the condenser aperture makes better use of dose, since there is no masking of the beam by apertures further downstream, and it allows a range of magnifications to be programmed simply by adjusting the condenser lens settings, rather than inserting different sized apertures in the SAA strip. A further significant difference here is the use of an amplitude diffuser instead of a phase diffuser. With the phase diffuser, a silicon nitride membrane with a random thickness profile introduced variable phase delays into the electron beam to produce a randomly structured illumination profile; the amplitude diffuser similarly structures the illumination, without introducing additional contrast-reducing inelastic background into the data. It is composed of 350 nm-wide, randomly arranged tracks within a 50 μm silicon nitride aperture, as shown in Fig. 1(b). The electrons either pass freely through the vacuum, or they are completely blocked by the tracks, such that the slightly defocused image of the condenser aperture incident on the sample contains a pattern of fringes and phase distortions, as shown in the reconstructed probe phase images of Fig. 2. (Note that large-scale phase aberrations introduced by the condenser optics are also present in the probe beam.)

We trialed the experimental configuration shown in Fig. 1 on the Cs-corrected Titan HOLO electron microscope at the Ernst-Ruska Center, Forschungszentrum Juelich GmbH, Germany. The microscope
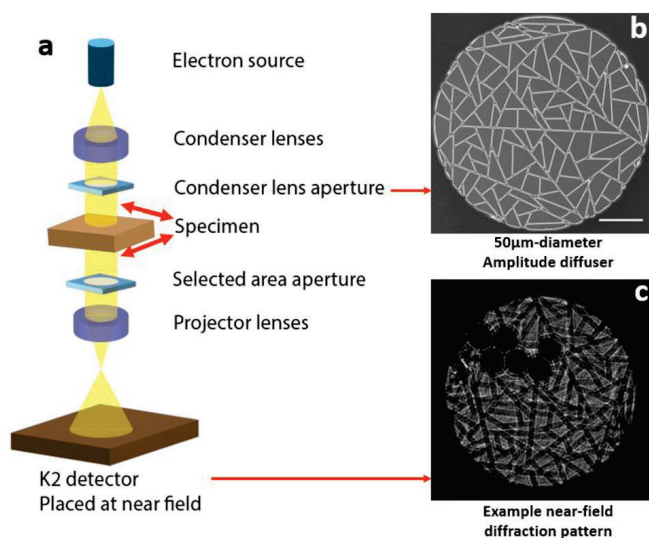

FIG. 1. The experiment setup of near-field electron Lorentz ptychography. (a) A schematic of the experimental arrangement; the objective lenses are turned off, and a parallel illumination probe, including features projected from the amplitude diffuser, shown in (b), illuminates the sample. The translation of the sample is indicated by the red arrows. (b) The amplitude diffuser inserted at the condenser lens aperture (scale bar: 10 μm). (c) An example near-field diffraction pattern with latex spheres as the sample.

was operated at 300 keV with a spot size of 3, in Lorentz mode with the objective lens turned off for a field-free sample environment (although the microscope geometry we describe is equally applicable to conventional brightfield TEM phase imaging with the objective lens on). The HOLO microscope is equipped with two electron biprisms optimized for flexible field of view off-axis electron holography measurements, which we employed for comparative measurements, and a Gatan K2 detector with 3840×3712 pixels on a 5 μm pitch. For the ptychography experiments, the sample was translated using the stepper motor stages on the sample holder, programmed via Digital Micrograph scripts. The central 2048×2048 pixels were extracted from each diffraction pattern, and the data were binned by 2 to mitigate the computation burden during reconstruction and reduce noise. The exposure time was 0.1s. Under the K2 linear mode, each dataset of 100 diffraction patterns took 5 minutes to collect—the bulk of this time being used for moving and settling the sample stage.

Our initial experiments used a test sample comprising a 463 nm gold-shadowed carbon diffraction grating replica populated with polystyrene spheres of 263 nm diameter, as in previous papers.[16,17] With these tests, the ability to tune the illumination size and magnification was demonstrated. Further experiments attempted phase imaging of a Mo-doped Permalloy magnetic sample, with results compared to off-axis electron holography on the same microscope. For the initial experiments, the microscope condenser lenses were tuned such that out-of-focus images of the amplitude diffuser and condenser aperture were projected onto the carbon replica sample with diameters of 1 and 2 μm. The microscope projection lenses were adjusted to a defocus of 982 μm and a magnification of 7632 for the 1 μm experiment, and a defocus of 952 μm and a magnification of 3562 for the 2 μm experiment. The resulting diffraction patterns are exemplified by Fig. 1(c). The sample was scanned in a raster fashion through a grid of 10×10 positions with a step size of 20% of the corresponding illumination diameter. The data were reconstructed using a modified version of the "ePIE" algorithm, as described in Ref. 16. The algorithm modifications compensate for experimental noise and uncertainty, including inelastic scatter, inaccurate scan positions, and a slow drift of the diffraction pattern center during data collection. This drift was roughly corrected via cross correlation in a pre-processing step, before 1000 iterations of the algorithm were carried out.

The reconstructed sample images are shown in Fig. 2(a) (1 μm illumination) and Fig. 2(d) (2 μm illumination). The illumination wavefronts are reconstructed by our algorithm along with the sample images and are shown in Figs. 2(b), 2(c), 2(e), and 2(f). A Fourier Ring Correlation (FRC) was used to assess the resolution of our results. To do this, the diffraction patterns from each experiment were split into two subsets (the odd and even patterns), and two independent reconstructions generated. The FRC was calculated from the 600×600 pixels central area of the two resulting phase images. The half-bit threshold, which was used as a resolution measure, intersected the FRC curve at a frequency of 0.1879 nm^{-1} for the 1 μm illumination data and at a frequency of 0.0982 nm^{-1} for the 2 μm illumination data, corresponding to resolutions of 5.32 and 10.18 nm, respectively.

Our second set of experiments compared the imaging of a Mo-doped Permalloy magnetic sample via our method with a benchmark result from off-axis electron holography. The same setup shown in Fig. 1 was employed, with the 2 μm-diameter illumination. The projection lenses were adjusted to give a defocus of 952 μm and a
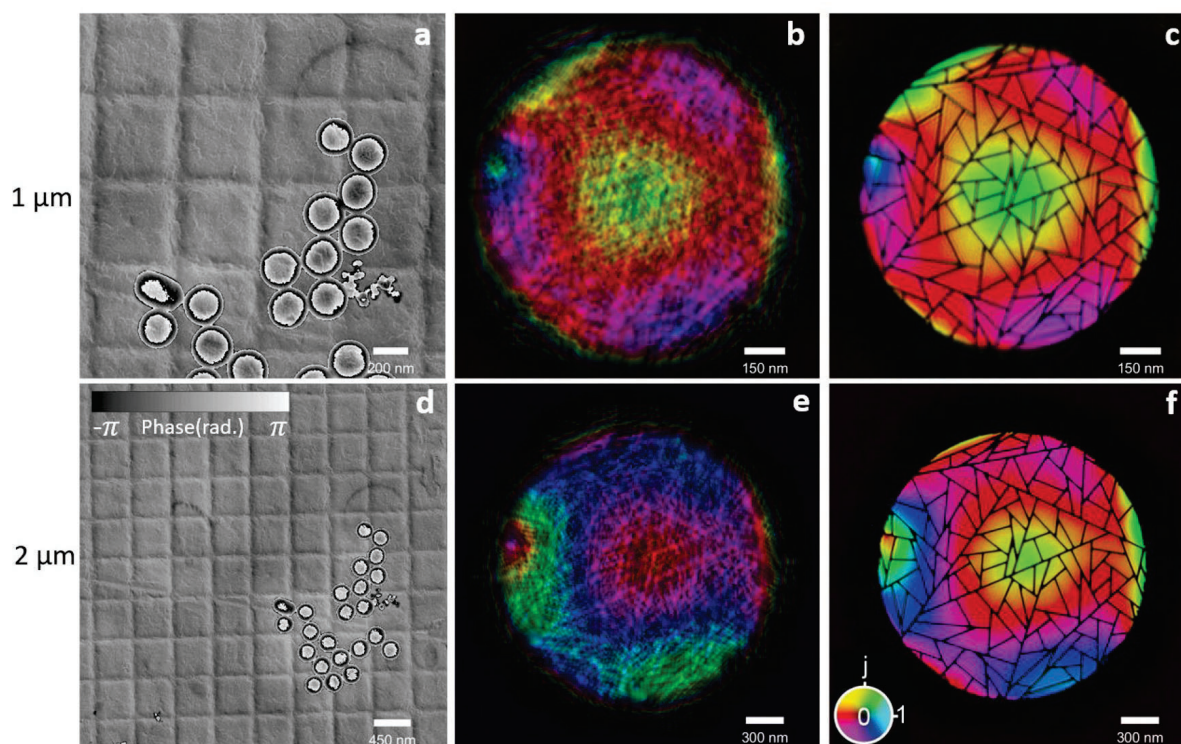
FIG. 2. Reconstructed latex sphere sample and the corresponding illumination probe. (a) and (d) The unwrapped phase of the reconstructed latex sphere sample under 1 and 2 μm diameter illumination, respectively. (b) and (e) The reconstructed illumination wavefronts on a colorwheel scale. (c) and (f) The same wavefronts back-propagated to the condenser aperture plane.

magnification of 3562. The sample was scanned through a 10×10 grid of positions with a step size of 10% of the illumination size, which produced a more reliable reconstruction in this case. Results are shown in Fig. 3(a) (modulus) and Fig. 3(c) (phase). Since the objective lens is turned off and the sample is of uniform thickness, the phase signal in Fig. 3(c) is predominantly governed by variations in magnetic field,[18] and the gradient of the phase is proportional to the in-plane magnetic induction of the sample. A set of comparative off-axis holography data were also collected, using the same TEM settings, to assess the accuracy of the ptychography phase reconstruction. The holographic reconstructions are shown in Fig. 3(b) (modulus) and Fig. 3(d) (phase). The methods show a good match in both modulus and phase. To accurately compare the phase images, the ptychographic reconstruction was carefully registered to the hologram, to account for slightly different rotation and magnification, a small shift in astigmatism, a global phase offset, and different sample positioning within each field of view. The area indicated by the red square in Fig. 3(c) was cut out from the two images and the phase unwrapped. The phase difference between these unwrapped areas (the unwrapped hologram phase minus the unwrapped ptychographic phase) is shown in Fig. 4. Several dots, such as that indicated by the red circle, arise from artifacts in the hologram caused by dead or occluded detector pixels. Fringes at the bottom, indicated by the red oval, correspond to biprism fringes at the edge of the hologram field of view. It is interesting to note the difference in the vacuum region outside of the sample; it is not clear from our results which method accurately represents the true phase in this region. Apart from these features,
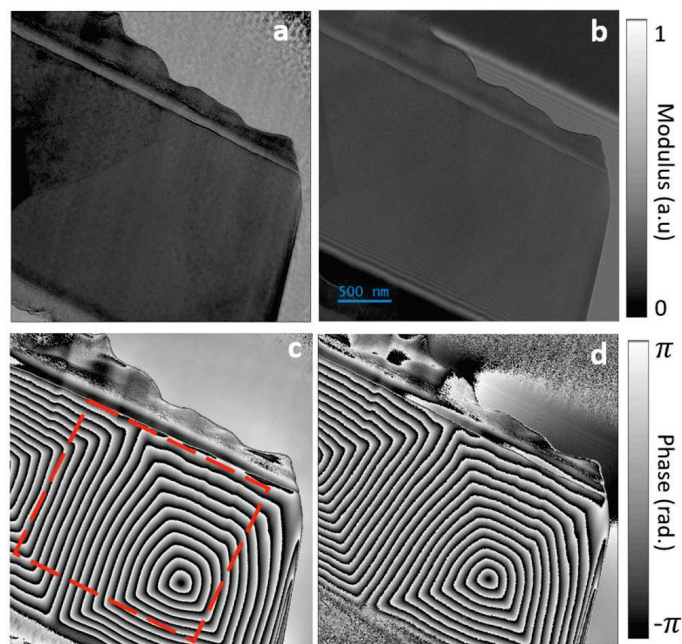

FIG. 3. Reconstructed images of a Mo-dope Permalloy sample obtained by ptychography and holography. (a) The modulus and (c) the phase of the ptychographic reconstruction; (b) the modulus and (d) the phase of the hologram. The phase shifts in (c) and (d) are primarily caused by variations in the sample's in-plane magnetic field. The region indicated by the red square is used to further analyze the accuracy of the phase reconstruction, as shown in Fig. 4.
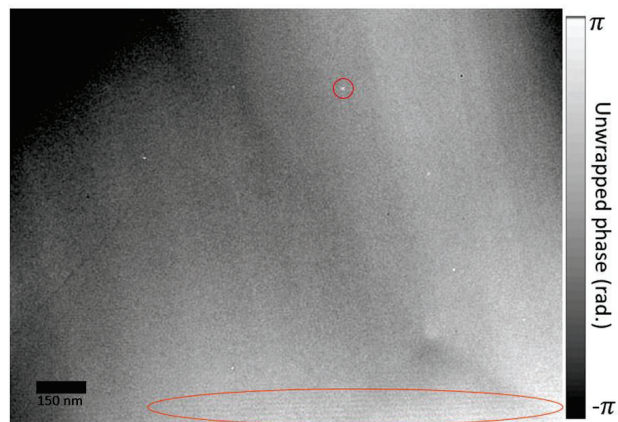
FIG. 4. The difference between the unwrapped ptychographic and holographic phase images within the area indicated by the red square in Fig. 3(c) (i.e., the unwrapped ptychographic phase image subtracted from the unwrapped holographic phase). The red circle identifies one of several dead or occluded detector pixels that appear in the hologram but not in the ptychographic reconstruction. The red oval highlights fringes from the biprism at the edge of the hologram field of view.

the central areas show close agreement—less than a phase wrap of variation over the entire magnetic domain.

In this Letter, we demonstrated an improved implementation of near-field electron ptychography using an amplitude diffuser positioned in the condenser aperture strip. Unlike previous implementations, variable magnifications are possible in this geometry, via appropriate adjustment of condenser and projection lens settings; more efficient use of dose is ensured because there are no post-specimen apertures, and the amplitude diffuser reduces inelastic scatter compared to previous phase diffusers. Our results show good agreement with off-axis holography. The ptychographic method benefits from a comparatively simple experimental setup, a readily extended field of view and no requirement for a vacuum reference adjacent to the sample. Holography is quicker in terms of data collection and processing and is unaffected by inelastic scatter. The major objective of further development in this area is to investigate the spatial resolution limit. To reach atomic resolution would require an illumination size much smaller than the $1\,\mu$m used here and would, therefore, require a step size smaller than the minimum possible with the stepper motor stage. Hence, a more efficient scanning approach is required, perhaps using the beam shift coils or a piezo-driven stage. Both alternatives would also speed up data collection, which would compensate for stage drift. Since dose efficiency should be improved in this configuration, another objective is to investigate the capability of near-field electron ptychography for imaging beam sensitive samples.

AUTHOR DECLARATIONS
Conflict of Interest

The authors have no conflicts to disclose.

Author Contributions

Shengbo You and Peng-Han Lu contributed equally to this work.

Shengbo You: Conceptualization (equal); Data curation (equal); Formal analysis (equal); Investigation (equal); Methodology (equal); Validation (equal); Visualization (equal); Writing – original draft (equal); Writing – review & editing (equal). **Peng Han Lu:** Conceptualization (equal); Data curation (equal); Investigation (equal); Methodology (equal); Writing – review & editing (equal). **Thomas Schachinger:** Resources (lead). **András Kovács:** Resources (equal). **Rafal Dunin-Borkowski:** Conceptualization (equal); Funding acquisition (equal); Supervision (equal); Writing – review & editing (equal). **Andrew Maiden:** Conceptualization (equal); Funding acquisition (equal); Supervision (equal); Writing – review & editing (equal).

DATA AVAILABILITY

The data that support the findings of this study are available from the corresponding author upon reasonable request.

REFERENCES

[1] J. Rodenburg and A. Maiden, "Ptychography," *Springer Handbook of Microscopy* (Springer, Cham, 2019), pp. 819–904.

[2] G. Zheng, R. Horstmeyer, and C. Yang, "Wide-field, high-resolution Fourier ptychographic microscopy," Nat. Photonics **7**, 739–745 (2013).

[3] L. Wiggins, A. Lord, K. L. Murphy, S. E. Lacy, P. J. O'Toole, W. J. Brackenbury, and J. Wilson, "The CellPhe toolkit for cell phenotyping using time-lapse imaging and pattern recognition," Nat Commun. **14**, 1854 (2023).

[4] P. Thibault, M. Dierolf, A. Menzel, O. Bunk, C. David, and F. Pfeiffer, "High-resolution scanning x-ray diffraction microscopy," Science **321**, 379–382 (2008).

[5] J. M. Rodenburg, A. Hurst, A. G. Cullis, B. R. Dobson, F. Pfeiffer, O. Bunk, C. David, K. Jefimovs, and I. Johnson, "Hard-x-ray lensless imaging of extended objects," Phys. Rev. Lett. **98**, 034801 (2007).

[6] F. Pfeiffer, "X-ray ptychography," Nat. Photonics **12**, 9–17 (2018).

[7] M. Humphry, B. Kraus, A. Hurst, M. A. M, and J. M. Rodenburg, "Ptychographic electron microscopy using high-angle dark-field scattering for sub-nanometre resolution imaging," Nat Commun **3**, 730 (2012).

[8] H. Yang, R. Rutte, L. Jones, M. Simson, R. Sagawa, H. Ryll, M. Huth, T. Pennycook, M. Green, H. Soltau *et al.*, "Simultaneous atomic-resolution electron ptychography and Z-contrast imaging of light and heavy elements in complex nanostructures," Nat. Commun. **7**, 12532 (2016).

[9] Y. Jiang, Z. Chen, Y. Han, P. Deb, H. Gao, S. Xie, P. Purohit, M. W. Tate, J. Park, S. M. Gruner *et al.*, "Electron ptychography of 2D materials to deep sub-ångström resolution," Nature **559**, 343–349 (2018).

[10] Z. Chen, Y. Jiang, Y.-T. Shao, M. E. Holtz, M. Odstrčil, M. Guizar-Sicairos, I. Hanke, S. Ganschow, D. G. Schlom, and D. A. Muller, "Electron ptychography achieves atomic-resolution limits set by lattice vibrations," Science **372**, 826–831 (2021).

[11] L. Zhou, J. Song, J. S. Kim, X. Pei, C. Huang, M. Boyce, L. Mendonça, D. Clare, A. Siebert, C. S. Allen *et al.*, "Low-dose phase retrieval of biological specimens using cryo-electron ptychography," Nat. Commun. **11**, 2773 (2020).

[12] C. Ophus, "Four-dimensional scanning transmission electron microscopy (4D-stem): From scanning nanodiffraction to ptychography and beyond," Microsc. Microanal. **25**, 563–582 (2019).

[13] M. Stockmar, P. Cloetens, I. Zanette, B. Enders, M. Dierolf, F. Pfeiffer, and P. Thibault, "Near-field ptychography: Phase retrieval for inline holography using a structured illumination," Sci. Rep. **3**, 1927 (2013).

[14] R. M. Clare, M. Stockmar, M. Dierolf, I. Zanette, and F. Pfeiffer, "Characterization of near-field ptychography," Opt. Express **23**, 19728–19742 (2015).

[15]W. Xu, H. Lin, H. Wang, and F. Zhang, "Super-resolution near-field ptychography," Opt. Express **28**, 5164–5178 (2020).

[16]A. Maiden, M. Sarahan, M. Stagg, S. Schramm, and M. Humphry, "Quantitative electron phase imaging with high sensitivity and an unlimited field of view," Sci. Rep. **5**, 14690 (2015).

[17]F. Allars, P.-H. Lu, M. Kruth, R. E. Dunin-Borkowski, J. M. Rodenburg, and A. M. Maiden, "Efficient large field of view electron phase imaging using near-field electron ptychography with a diffuser," Ultramicroscopy **231**, 113257 (2021).

[18]P. Midgley, "An introduction to off-axis electron holography," Micron **32**, 167–184 (2001).